rjm00 | ACSJCA | JCA11.2.5208/W Library-x64 | manuscript.3f (R5.1.i4:5009 | 2.1) 2021/10/27 08:51:00 | PROD-WS-121 | rq_2751470 | 1/19/2022 17:03:10 | 8 | JCA-DEFAULT

THE JOURNAL OF PHYSICAL CHEMISTRY LETTERS
A JOURNAL OF THE AMERICAN CHEMICAL SOCIETY

pubs.acs.org/JPCL

Letter

Multi-reward Reinforcement Learning Based Bond-Order Potential to Study Strain-Assisted Phase Transitions in Phosphorene

Aditya Koneru,[⊥] Rohit Batra,* Sukriti Manna,[⊥] Troy D. Loeffler, Henry Chan, Michael Sternberg, Anthony Avarca, Harpal Singh, Mathew Cherukara, and Subramanian K. R. S. Sankaranarayanan*

Cite This: https://doi.org/10.1021/acs.jpclett.1c03551

Read Online

ACCESS | Metrics & More | Article Recommendations | Supporting Information

ABSTRACT: We introduce a multi-reward reinforcement learning (RL) approach to train a flexible bond-order potential (BOP) for 2D phosphorene based on ab initio training data sets. Our approach is based on a continuous action space Monte Carlo tree search algorithm that is general and scalable and presents an efficient multiobjective optimization scheme for high-dimensional materials design problems. As a proof-of-concept, we deploy this scheme to parametrize multiple structural and dynamical properties of 2D phosphorene polymorphs. Our RL-trained BOP model adequately captures the structure, energetics, transformation barriers, equation of state, elastic constants, and phonon dispersions of various 2D P polymorphs. We use this model to probe the impact of temperature and strain rate on the phase transition from black (α-P) to blue phosphorene (β-P) through molecular dynamics simulations. A decrease in critical strain for this phase transition with increase in temperature is observed, and the underlying atomistic mechanisms are discussed.

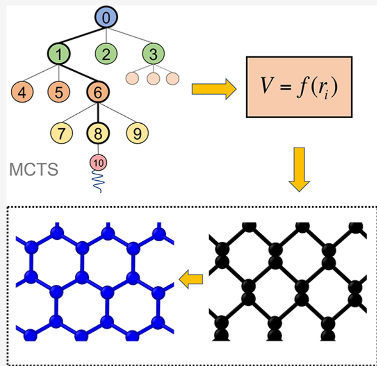

Phosphorene, a recently discovered 2D analogue of bulk phosphorus, has generated a tremendous amount of excitement owing to their unique physicochemical and electronic properties, and structural features[1] that include its puckered layered structure. In particular, it presents a widely tunable band gap, strong in-plane anisotropy, and high carrier mobility,[2−5] which make it an exciting material of choice for emerging electronic, optoelectronic, and spintronic applications.

There are several polymorphs of phosphorene, each of which can have a significant variation in their physical, chemical, electronic, and mechanical properties. Two most notable polymorphs of phosphorene are the black (α-P)[6] and blue (β-P)[7] phosphorene that are known for their tunable band gap, which is usually modulated by varying the number of layers or the applied strain. Their band gap can be tuned over a much larger regime of 0.3−2.0 eV, as compared to other counterparts such as WSe_2 and MoS_2 for which this value ranges around 1.2−1.8 eV. Moreover, heterostructures that comprise graphene/phosphorene stacking have resulted in a much wider band gap ranging from 0.004 to 4.26 eV.[8] The α-P and β-P polymorphs have been explored in the areas of chemical catalysis, detectors, and photocatalytic reactions.[9,10] Given the wide variation in the polymorph properties of 2D phosphorene—black is semiconducting, whereas blue can be metallic—there has been a lot of effort focused on engineering the phase transformation to exercise better control over phenomena such as electron−phonon coupling enhancement,[11] superconductivity,[12] semiconductor to metal transition,[13] band gap modification,[14] and direct−indirect band gap transition.[15] Strain engineering or applications of pressure represents one of the viable routes to modify the structure and thereby the properties of 2D phosphorene.[16]

Several recent theoretical studies, primarily based on first-principles calculations, have explored the effect of strain on the electronic structure of single- and/or few-layer phosphorene. For example, density functional theory (DFT) calculations[17] of a few-layer (one to five layers) α-P suggest that compressive strain can lead to a semiconductor−metal transition. On the other hand, the biaxial tensile strain was found to only affect the band gaps and does not alter other electronic properties of the system. In another study[18] a reversible semiconductor−metal transition was observed at ∼13% of normal compressive strain that was attributed to the strong interlayer interactions between the phosphorus p_z orbitals. The authors also found a direct−indirect band gap transition at ∼3% of strain suggesting that strain can engineer property modulation structural modifications.

There are several other unique properties including mechanical properties that are also of significant interest. For example, phosphorene can sustain tensile strains over 30%—which is higher than that reported for graphene[19] or single-layer MoS_2.[20] The puckered structure results in a negative

Received: October 29, 2021
Accepted: January 18, 2022

Table 1. RL Optimized BOP Model (Tersoff) Parameters of Phosphorene Obtained in This Work

m	γ	λ_3 (Å^{-1})	c	d	θ	n
1	0.883338	0.873251	86567.3351	222.44853	−0.269673	0.80808
β	λ_2 (Å^{-1})	B (eV)	R (Å)	D (Å)	λ_1 (Å^{-1})	A (eV)
0.783731	1.184091	69.693302	2.540076	0.114989	3.584868	1902.96888

Poisson ratio, higher ductility in the AM (armchair) direction compared to the ZZ (zigzag) direction and good mechanical flexibility.[21] These studies clearly indicate the importance of understanding structure−property relationships in phosphorene polymorphs. More importantly, while there has been a significant amount of computational effort, most have primarily involved the use of first-principles calculations based on DFT. Dynamical studies that aim at understanding the structural and phase transformation upon application of external stimuli (such as mechanical,[22] thermal,[23,24] etc.) over time (picoseconds to microseconds) and length scales (≫tens of nanometers) are of significant importance. In this respect, classical molecular dynamics (MD) simulations represent an excellent approach to address this challenge.

It is not surprising that there have been significant efforts on developing high-quality interatomic potentials for phosphorene. Some notable classical potential models include the Stillinger−Weber (SW)[25] potential to individually model α-P and β-P phases, with a model for the α-P phase that consists of two separate atom types. There is a parametrization of ReaxFF[26] that is capable of modeling both the black and blue polymorphs, but their stress−strain curves erroneously display no indication of phase transition. There have been a few qualitative reports on a possible transition from α-P to β-P[27] as a part of mechanical property evaluation. A recently developed machine learning based Gaussian approximation potential[28] (GAP) is trained on a very diverse data set of P configurations representing a model capable of making predictions across several polymorphs of P, but its high quality comes at a greater computational expense in comparison to its analytical counterparts. It is highly desirable to develop accurate but fast interatomic potentials for performing dynamical simulations of materials.

Traditionally, the development of these potential models, including those based on machine learning, involve navigation through a high-dimensional parameter space and remain nontrivial. Briefly, local optimization techniques rely on gradient based information (which require well-defined gradients of the objective function). While this approach can be efficient, it is limited in terms of the search space explored. In contrast, the global optimization techniques, such as those based on genetic algorithms,[29] particle swarm,[30] or Bayesian optimization,[31] explore a wider search space and thus have been successful. However, their performance both in terms of the solution quality and the number of evaluations to reach an optimal solution tends to be poor in higher dimensional search spaces. This is further complicated when one is dealing with multiple objectives—the search algorithms tend to be biased depending on the choice of weights or are dependent on the user (pareto-type) to choose from the pareto front.

Here, we introduce a multi-reward reinforcement learning (RL) workflow (Figure 5) that allows us to efficiently navigate through a high-dimensional parameter space involving a multiple set of objectives. To circumvent the issues with the choice of the weights, we introduce the concept of multiple rewards arranged in a hierarchical level within the framework of a continuous action space RL algorithm such as Monte Carlo tree search (MCTS). We apply it to a representative problem of multiobjective potential parameter optimization to develop a computationally cheap yet efficient bond-order potential (BOP) model for phosphorene polymorphs. We chose the BOP formalism since it involves navigating through a relatively complex 14-dimensional space (please see the Supporting Information), but the output potential model is efficient enough to simulate longer time-scale and larger length-scale simulations to study strain-induced phase transition between α-P and β-P.

Using the multi-reward RL workflow, we obtain optimal model parameters shown in Table 1. To assess the model accuracy, we compare its predictions against those in the training set obtained through DFT calculations. The results are presented in Table 2. We find that the relative error in lattice

Table 2. Lattice Parameters and Cohesive Energies of Different Polymorphs of Phosphorene Obtained Using DFT and BOP (Tersoff) Potential

phase	α-P		β-P	
method	DFT	BOP	DFT	BOP
a (Å)	3.326	3.273	3.296	3.273
b (Å)	4.573	4.315	3.296	3.273
γ (deg)	90.000	90.000	60.00	60.00
E_{coh} (eV/atom)	−3.4799	−3.6742	−3.4804	−3.6742
C_{11} (GPa)	44.9138	27.6464	35.7721	22.5312
C_{12} (GPa)	8.4114	0.024	3.8423	3.3804
C_{22} (GPa)	10.9772	4.9874	35.765	22.5312

parameters prediction is less than 8% for the different polymorphs, while the errors in energetics are less than 6%. We note that it is quite difficult to optimize potentials when the different polymorphs have almost identical cohesive energies. Our potential, however, simultaneously captures the properties and energetics of both the α and β phases accurately, even though both phases have near-identical energies. The relative energetic ordering of different polymorphs is in excellent agreement with that of DFT computations. Note (see Table 2) that the polymorphs investigated in this work for strain-induced phase transition, i.e., α-P and β-P, are predicted with much lower errors in comparison to the higher energy or non-equilibrium monoclinic (θ-P) polymorph.

Our model accurately reproduces the shape of the equation of state (EOS) curve for the different polymorphs and our elastic constant predictions are in good agreement with that from the first-principles calculations (Figure 1a and Table 2). We further compare the phonon dispersion curves predicted across the different polymorphs (Figure 1b) by the model with respect to those obtained from DFT. The model predictions are in excellent agreement with those from DFT calculations in terms of both shape and magnitude.

A clear crossover could be seen in the strained configurations at 0 K (Figure 2), which suggests that the

https://doi.org/10.1021/acs.jpclett.1c03551
J. Phys. Chem. Lett. XXXX, XXX, XXX−XXX

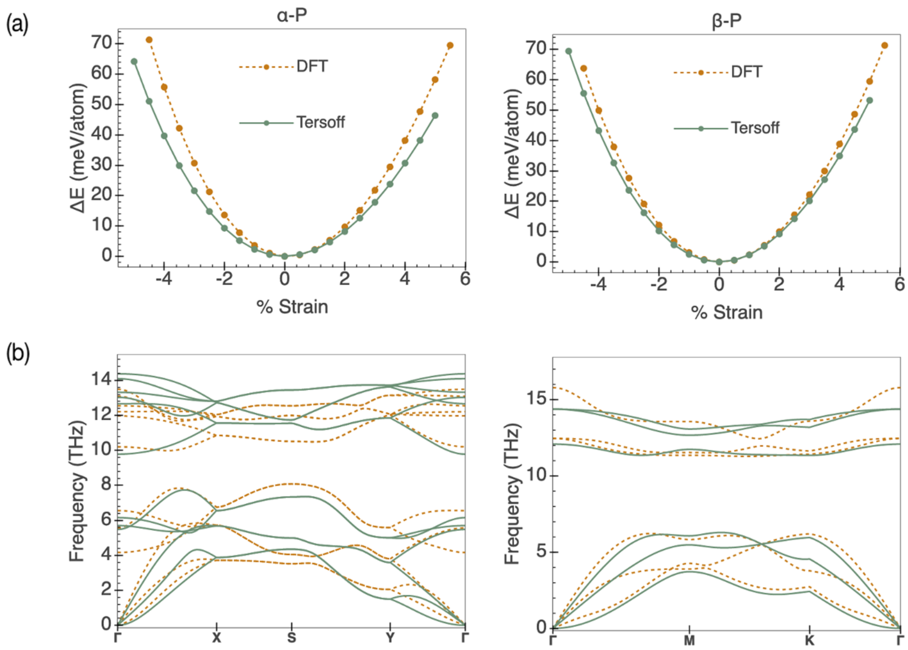

Figure 1. (a) Equation of state (EOS) and (b) phonon dispersion behavior of different polymorphs of phosphorene as obtained using the reference DFT and the trained BOP (Tersoff) model in this work. In panel a, the energy is relative to the relaxed configuration with no strain.

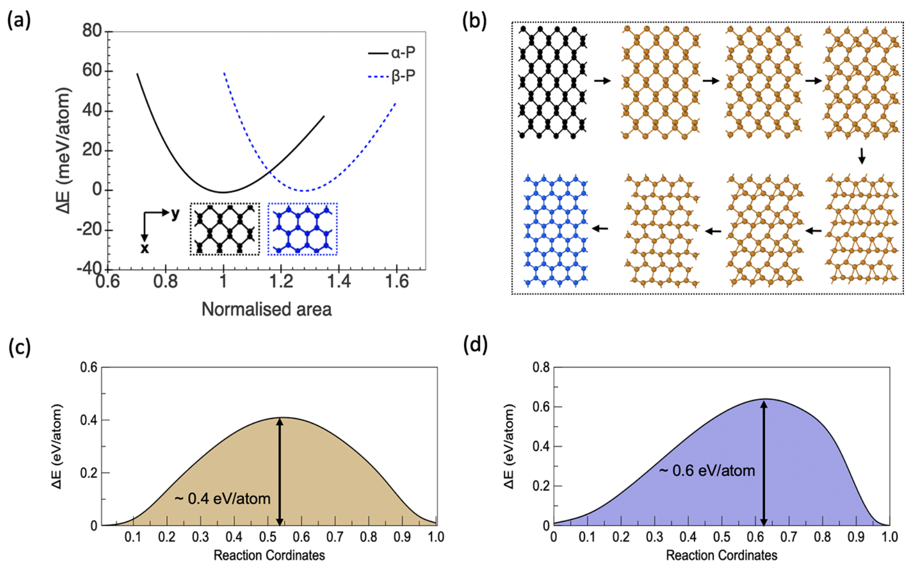

Figure 2. (a) Energy of α-P and β-P phosphorene as a function of strain at 0 K as obtained using the Tersoff model. The sheet area and energy are referenced with respect to those of relaxed α-P phosphorene. (b) Few transition snapshots obtained using DFT evaluations. Energy barrier for phase transition from α-P to β-P using (c) DFT and (d) BOP (Tersoff) model.

model EOS can adequately represent the strain-assisted phase transformation across these two polymorphs. We next compare the energy barrier for transformation between α-P and β-P polymorphs obtained by the BOP model and DFT using the climbing image nudged elastic band calculations (please see Supporting Information Section S1.4).[32,33] The barrier between black and blue phosphorene phases along with the minimum energy pathway and saddle point was obtained from climbing image nudged elastic band (CI-NEB) calculations. Figure 2b shows the various NEB images that depict the transition states, whereas panels c and d of Figure 2 show the barriers for transformation between α-P and β-P polymorphs computed using DFT and the RL-trained BOP model, respectively. We find that the barriers are in good agreement (0.4 eV for DFT vs 0.6 eV for BOP) which allows us to now explore the use of strain to overcome this barrier and possibly control the phase transition.

We next deploy our RL-trained BOP model and perform MD simulations to investigate the strain-assisted phase transition at different temperatures from 10 to 500 K (see Methods for more details). For brevity, we limit the discussion to the case of 300 K, while the results for other temperatures are provided in the Supporting Information. Starting from the black (α-P) phosphorene at various temperatures, the configuration was strained along [010] at a rate of 1×10^{-6} ps^{-1} until the 2D sheet reaches failure. Figure 3a showcases the stress−strain curve obtained from the simulations. Interestingly, the curve comprises multiple slopes unlike that of a

https://doi.org/10.1021/acs.jpclett.1c03551
J. Phys. Chem. Lett. XXXX, XXX, XXX−XXX

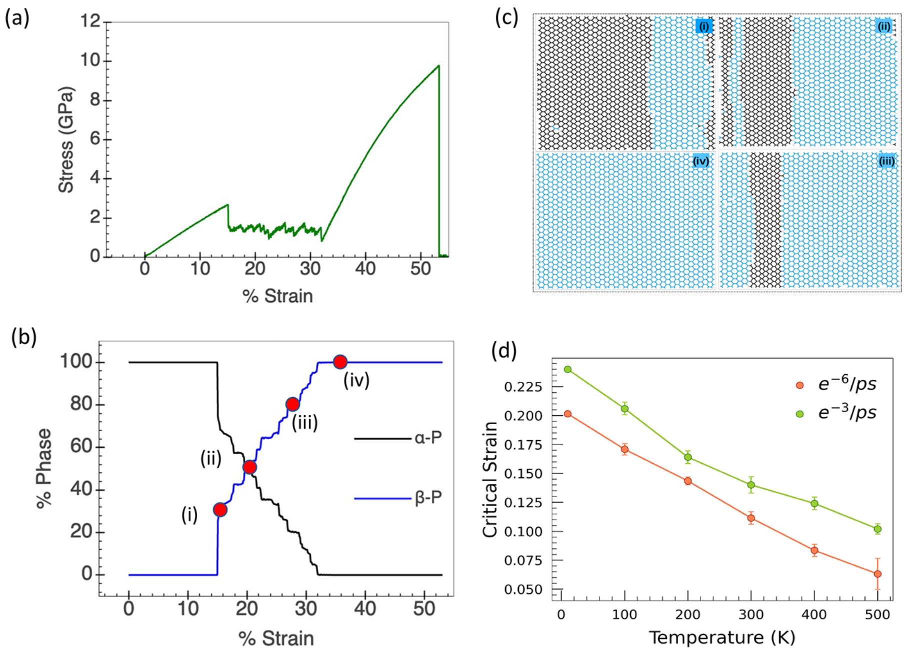

Figure 3. Phase transformation in phosphorene due to uniaxial strain at 300 K. (a) Observed stress vs strain behavior, (b) fraction of α-P/intermediate-P/β-P computed using the SOAP fingerprint analysis. (c) Associated (i), (ii), (iii), and (iv) demonstrating representative structures during the transformation, with black/white/blue color highlighting the α-P/intermediate/β-P phase to which each P atom belongs. (d) Temperature and strain-rate dependence of uniaxial strain at which α-P to β-P phase transformation was observed using the MD simulations. Error bars indicate 2σ standard deviation from five independent simulations.

typical single-phase stress−strain curve; the stress reduces around 14% strain and remains relatively flat until 32% strain, when, subsequently, it begins to increase, although with a different slope this time, until it drops to zero at 53% strain, marking the failure of the 2D sheet. With a continuous injection of strain energy into the system at isothermal conditions, one would expect a monotonic increase in stress until the yield point, but the observed behavior is remarkably different.

This suggests that the strain energy leads to a change in atomic rearrangement, indicating phase transition prior to failure. Representative snapshots shown in Figure 3c confirm the presence of multiple competing phases. To obtain a more quantitative distribution of the α-P and the β-P phases during the MD trajectory, we use an atomic fingerprinting analysis. The observed transition is continuous and leads to mixed blue/black/intermediate defective phases before the complete transformation to pure phase.

To determine the phase distribution of the phosphorene during the applied uniaxial strain, an atomistic fingerprinting technique was used. We use the smooth overlap of atomic positions (SOAPs) fingerprint (105-dimensional unique SOAP fingerprint vector for each atom). The cosine distance was computed and compared against those of atoms in pure blue and black phosphorene. The smaller the cosine distance of an atom fingerprint to that of the black (or blue) phosphorene, the more likely it is that the atom belongs to the black (or blue) phosphorene phase. With this definition, we characterized each atom in a simulated trajectory as either blue, black, or intermediate and studied their dynamical evolution (see Figure 3b).

Comparing Figure 3a,b, we note that the 25% rise in β-P phase corresponds to the decrease in stress around 14% strain. With additional strain, the system completely transforms into 100% α-P phase matching the change in the slope of the stress−strain curve at 32% strain. This can both be visually confirmed from the snapshots (Figure 3c) and also the phase distribution plot. Additionally, the slopes quantitatively depict a higher elastic modulus for the β-P phase which qualitatively agrees with the values predicted both by DFT and the BOP model (see Table 2). Therefore, the transition behavior has been verified both visually[34] and analytically.

Next we show that the above strain-induced phase transition in phosphorene can be tuned with a change in temperature and applied strain rate—this is relevant especially for materials employed in optoelectronic applications. Temperature effect on the critical strain needed for the onset of phase transition from black (α-P) to blue (β-P) phosphorene as a function of temperature is presented in Figure 3d. The critical strain needed for phase transition is inversely related with the temperature. While at extremely low temperatures (~10 K) about 20% strain is needed to initiate the formation of β-P phase, this value drops to only 6% at 500 K. This inverse relation is expected as with increasing temperature thermal energy also assists in overcoming the transition energy barrier captured in Figure 2. Similarly, an increase in the strain rate can be observed to increase the critical strain necessary to initiate phase transition; compare red and green curves in Figure 3d. This again can be understood from kinetic effects as at lower strain rate the system has more time to jump over the transition barrier. (Also the effect of temperature on strain to failure can be noted in the Supporting Information from Figures S5 to S9. These results provide theoretical estimates and lay the groundwork for experimentalists to tune the operating conditions required to control the α-P to β-P phase transition.

Density functional theory can accurately capture diverse bonding environments within a single formulation—this allows

https://doi.org/10.1021/acs.jpclett.1c03551
J. Phys. Chem. Lett. XXXX, XXX, XXX−XXX

it to model both clusters and interfaces (reactive as well as nonreactive) to be captured. It is worth noting that the scalability of several available DFT codes have now made ab initio molecular dynamics (AIMD) simulations quite feasible. Despite this progress, there still remains a significant gulf between the spatiotemporal scales accessible to AIMD and classical molecular dynamics (MD) simulations that employ empirical physics based potentials. There have been several different potential models—the BOP formalism represents a simple and elegant way to capture both pair-wise and three-body interactions. Powerful high-quality ML models such as neural networks[35,36] (NN) or GAP[37] have emerged as a viable alternative to DFT—it is worth noting that ML models based on NN are interpolative and as such perform poorly outside of their training data set. GAP potentials represent an ML approach to derive interatomic potentials directly from data sets (energies and forces experienced by atoms) computed using quantum mechanical calculations. While they achieve a high degree of accuracy and are computationally much cheaper compared to DFT, their computational cost is still high compared to simpler physical models such as BOP. The BOP formalism is thus computationally much cheaper, but the main challenge lies in achieving high accuracy compared to DFT. If trained properly (as shown in this work), it has the ability to capture several diverse environments, allowing it to access time and length scales that extend to several 100s of nanometers and 100s of nanoseconds.

To illustrate this, we benchmark the RL-trained BOP model against state-of-the-art classical and ML models such as SW,[25] ReaxFF,[26] and GAP[28] (see the Supporting Information for details on the property comparison). For a fair comparison, all of the MD equilibration and production runs of different system sizes were carried out on a single CPU core. Figure 4

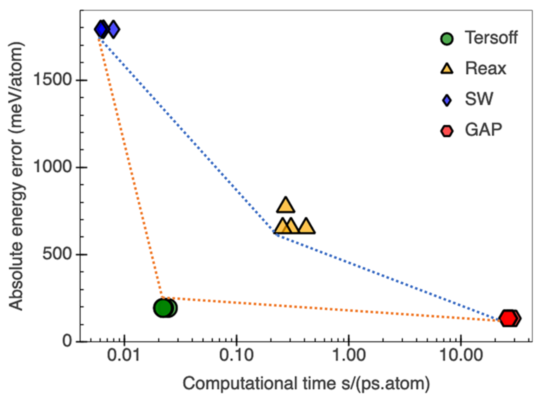

Figure 4. Computational cost vs accuracy. The orange and blue dashed lines denote the Pareto frontier. The models have been evaluated at different sizes, and the error has been reported against the target DFT values used to fit the model in this work.

shows that the size effects were insignificant relative to the computational cost of the different interatomic potentials; different points of the same shape indicate varying sizes. As expected, all the models are far apart when correlating cost with accuracy—we observe that ML models such as GAP[28] achieve high accuracy but also exhibit high computational cost. Both SW and BOP (Tersoff) are scalable owing to their low cost, but the SW model displays higher errors, perhaps due to limited flexibility in the functional form. On the other hand, the RL-trained BOP model has comparable accuracy to that of the GAP[28] model but at a significantly (about an order of magnitude) lower computational cost.

In summary, our multi-reward RL approach to develop high-fidelity yet computationally cheap BOP models opens up new opportunities for dynamical simulations of low-dimensional materials in the mesoscale regime, thereby accelerating their design and discovery.

■ METHODS

The MCTS tree consists of several nodes, each of which contains a unique BOP parameter set. The main idea is to grow those tree branches that contain nodes with promising parameter set. For this, the head node of the MCTS tree is initialized randomly with a BOP parameter set and then the four stages of MCTS are executed iteratively using a learning policy with modifications as outlined above. In the selection stage, the node with the highest score based on the learning policy is selected. Here, we use the popular upper confidence bound (UCB) as the learning policy, with important modifications to suit efficient optimization in the continuous potential energy surface as opposed to the traditional discrete design space. The learning policy contains two parts; one is focused on exploitation or achieving minimum error score, while the other is related to the exploration and is based on the ratio of parent to child node visits made by the MCTS agent. The latter term contains an exploration constant, a hyper-parameter that balances the exploitation vs exploration trade-off. Next, in the expansion stage, child nodes are added to the selected node such that their parameter values are small perturbations compared to that of the parent node. We note that the region of the space explored reduces with the increase in tree depth, which helps in the convergence of the algorithm.[38] In the simulation stage, playouts are conducted for the newly generated child nodes to evaluate their performance and the scores of all relevant parent and child nodes are updated in the back-propagation stage. The global optimization of the parameter sets is achieved through a multi-reward MCTS scheme which is followed by a Simplex algorithm[39] for subsequent local optimization to derive the final set of best parameters. The training data set derived from DFT computations are comprised of several different sets of objectives, which include structures of the various 2D phosphorene polymorphs and their energy, EOS, elastics, and phonon dispersion curves.

Analogous to computer games, we introduce a rewards scheme where the objectives are evaluated on the basis of a hierarchical manner where errors for multiple properties are evaluated stage-wise depending on the typically increasing level of difficulty (and/or are at the discretion of the user). All of the multiple objectives or rewards are evaluated using LAMMPS.[40] Initially, the agent makes a heuristic guess of the BOP parameters within the specified bounds of the high-dimensional space. The property evaluations are ordered according to their simulation cost, as demonstrated in Figure 5. The reward for the first stage (here lattice parameters) is evaluated, and if the constraint on the relative error is satisfied, the agent moves to evaluate the reward for the successive stages (cohesive energy, EOS, etc.) one at a time. The rewards from each stage are accumulated, and the overall reward is fed back to the agent. Thus, the reward value for a BOP parameter set is higher if it successfully completes multiple stages.

This approach offers a 2-fold advantage, one being early rejection of parameter sets without having to evaluate all of the

https://doi.org/10.1021/acs.jpclett.1c03551
J. Phys. Chem. Lett. XXXX, XXX, XXX−XXX

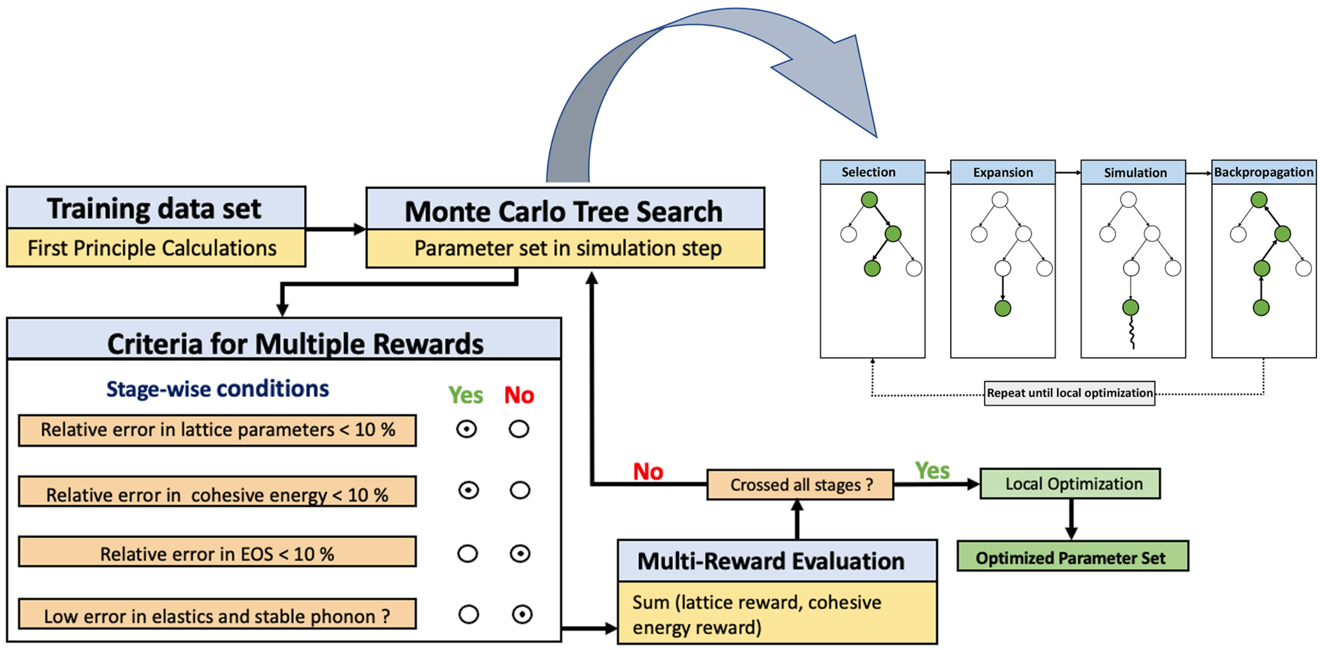

Figure 5. Multi-reward RL workflow to train BOP model for phosphorene. The training set consists of structure, energy, EOS, elastics, and phonon dispersions evaluated from DFT. The multi-reward technique gives the choice to tune the parameters on the basis of the relative importance of desired properties. The global optimization is performed using MCTS, while the parameter set satisfying all of the different stages of objectives is fed into a local optimizer like Simplex.

properties, thus saving time and computing power. The other is the ability to tune the search space to identify and map regions of good parameters relative to the most desired properties simultaneously. More details on the hyperparameters and the LAMMPS computations are provided in the Supporting Information.

■ ASSOCIATED CONTENT

Supporting Information

The Supporting Information is available free of charge at https://pubs.acs.org/doi/10.1021/acs.jpclett.1c03551.

More computational details, property comparisons across different interatomic potential models, effect of temperature on phase transition, and results from ongoing work on the development of BOP model for stanene (PDF)

■ AUTHOR INFORMATION

Corresponding Authors

Rohit Batra − *Center for Nanoscale Materials, Argonne National Laboratory, Lemont, Illinois 60439, United States;* orcid.org/0000-0002-1098-7035; Email: rohitbatra1989@gmail.com

Subramanian K. R. S. Sankaranarayanan − *Department of Mechanical and Industrial Engineering, University of Illinois, Chicago, Illinois 60607, United States; Center for Nanoscale Materials, Argonne National Laboratory, Lemont, Illinois 60439, United States;* orcid.org/0000-0002-9708-396X; Email: skrssank@uic.edu

Authors

Aditya Koneru − *Department of Mechanical and Industrial Engineering, University of Illinois, Chicago, Illinois 60607, United States; Center for Nanoscale Materials, Argonne National Laboratory, Lemont, Illinois 60439, United States;* orcid.org/0000-0002-6321-1900

Sukriti Manna − *Department of Mechanical and Industrial Engineering, University of Illinois, Chicago, Illinois 60607, United States; Center for Nanoscale Materials, Argonne National Laboratory, Lemont, Illinois 60439, United States;* orcid.org/0000-0002-3193-7803

Troy D. Loeffler − *Department of Mechanical and Industrial Engineering, University of Illinois, Chicago, Illinois 60607, United States; Center for Nanoscale Materials, Argonne National Laboratory, Lemont, Illinois 60439, United States;* orcid.org/0000-0003-0244-1793

Henry Chan − *Department of Mechanical and Industrial Engineering, University of Illinois, Chicago, Illinois 60607, United States; Center for Nanoscale Materials, Argonne National Laboratory, Lemont, Illinois 60439, United States;* orcid.org/0000-0002-8198-7737

Michael Sternberg − *Center for Nanoscale Materials, Argonne National Laboratory, Lemont, Illinois 60439, United States*

Anthony Avarca − *Center for Nanoscale Materials, Argonne National Laboratory, Lemont, Illinois 60439, United States*

Harpal Singh − *Research and Development, Sentient Science Corporation, West Lafayette, Indiana 47906, United States;* orcid.org/0000-0002-8726-2876

Mathew Cherukara − *Advanced Photon Source, Argonne National Laboratory, Lemont, Illinois 60439, United States;* orcid.org/0000-0002-1475-6998

Complete contact information is available at: https://pubs.acs.org/10.1021/acs.jpclett.1c03551

Author Contributions

⊥A.K. and S.M. contributed equally to this work.

Notes

The authors declare no competing financial interest.

■ ACKNOWLEDGMENTS

This work was supported by the U.S. Department of Energy through BES Award DE-SC0021201. This work was performed in part at the Center for Nanoscale Materials and the Advanced Photon Source, which are U.S. Department of Energy of Science User facilities supported by the U.S. Department of Energy, Office of Science, Office of Basic Energy Sciences, under Contract Nos. DE-AC02-06CH11357 and DE-AC05-00OR22725, respectively. We also acknowledge the LCRC computing facilities at Argonne.

■ REFERENCES

(1) Carvalho, A.; Wang, M.; Zhu, X.; Rodin, A. S.; Su, H.; Castro Neto, A. H. Phosphorene: From theory to applications. *Nat. Rev. Mater.* **2016**, *1* (11), 16061.

(2) Shao, D. F.; Lu, W. J.; Lv, H. Y.; Sun, Y. P. Electron-doped phosphorene: a potential monolayer superconductor. *EPL (Europhysics Letters)* **2014**, *108* (6), 67004.

(3) Luo, Z.; Maassen, J.; Deng, Y.; Du, Y.; Garrelts, R. P.; Lundstrom, M. S; Ye, P. D.; Xu, X. Anisotropic in-plane thermal conductivity observed in few-layer black phosphorus. *Nat. Commun.* **2015**, *6* (1), 8572.

(4) Yuan, H.; Liu, X.; Afshinmanesh, F.; Li, W.; Xu, G.; Sun, J.; Lian, B.; Curto, A. G; Ye, G.; Hikita, Y.; et al. Polarization-sensitive broadband photodetector using a black phosphorus vertical p−n junction. *Nat. Nanotechnol.* **2015**, *10* (8), 707−713.

(5) Low, T.; Rodin, A. S.; Carvalho, A.; Jiang, Y.; Wang, H.; Xia, F.; Castro Neto, A. H. Tunable optical properties of multilayer black phosphorus thin films. *Phys. Rev. B* **2014**, *90* (7), No. 075434.

(6) Liu, H.; Neal, A. T.; Zhu, Z.; Luo, Z.; Xu, X.; Tomanek, D.; Ye, P. D. Phosphorene: an unexplored 2D semiconductor with a high hole mobility. *ACS Nano* **2014**, *8* (4), 4033−4041.

(7) Zhu, Z.; Tomanek, D. Semiconducting layered blue phosphorus: A computational study. *Phys. Rev. Lett.* **2014**, *112* (17), 176802.

(8) Akhtar, M.; Anderson, G.; Zhao, R.; Alruqi, A.; Mroczkowska, J. E.; Sumanasekera, G.; Jasinski, J. B. Recent advances in synthesis, properties, and applications of phosphorene. *npj 2D Mater. Appl.* **2017**, *1* (1), 5.

(9) Rahman, M. Z.; Kwong, C. W.; Davey, K.; Qiao, S. Z. 2D phosphorene as a water splitting photocatalyst: Fundamentals to applications. *Energy Environ. Sci.* **2016**, *9* (3), 709−728.

(10) Fernández-Escamilla, H. N.; Guerrero-Sánchez, J.; Garcia-Diaz, R.; Martínez-Guerra, E.; Takeuchi, N. Adsorption of dimethyl sulfoxide on blue phosphorene. *Surf. Sci.* **2019**, *680*, 88−94.

(11) Profeta, G.; Tresca, C.; Sanna, A. Electron−phonon coupling in two-dimensional superconductors: Doped graphene and phosphorene In *GraphITA*; Springer, 2017; pp 31−45. DOI: 10.1007/978-3-319-58134-7_3.

(12) Ge, Y.; Wan, W.; Yang, F.; Yao, Y. The strain effect on superconductivity in phosphorene: A first-principles prediction. *New J. Phys.* **2015**, *17* (3), No. 035008.

(13) Arcudia, J.; Kempt, R.; Cifuentes-Quintal, M. E.; Heine, T.; Merino, G. Blue Phosphorene Bilayer is a Two-Dimensional Metal and an Unambiguous Classification Scheme for Buckled Hexagonal Bilayers. *Phys. Rev. Lett.* **2020**, *125* (19), 196401.

(14) Lu, J.; Wu, J.; Carvalho, A.; Ziletti, A.; Liu, H.; Tan, J.; Chen, Y.; Castro Neto, A. H.; Ozyilmaz, B.; Sow, C. H. Bandgap engineering of phosphorene by laser oxidation toward functional 2D materials. *ACS Nano* **2015**, *9* (10), 10411−10421.

(15) Peng, X.; Wei, Q.; Copple, A. Strain-engineered direct-indirect band gap transition and its mechanism in two-dimensional phosphorene. *Phys. Rev. B* **2014**, *90* (8), No. 085402.

(16) Galicia Hernandez, J. M.; Sanchez, J. G.; Fernandez Escamilla, H. N.; Cocoletzi, G. H.; Takeuchi, N. First-principles studies of the strain-induced band-gap tuning in black phosphorene. *J. Phys.: Condens. Matter* **2021**, *33* (17), 175502.

(17) Ju, W.; Li, T.; Wang, H.; Yong, Y.; Sun, J. Strain-induced semiconductor to metal transition in few-layer black phosphorus from first principles. *Chem. Phys. Lett.* **2015**, *622*, 109−114.

(18) Manjanath, A.; Samanta, A.; Pandey, T.; Singh, A. K Semiconductor to metal transition in bilayer phosphorene under normal compressive strain. *Nanotechnology* **2015**, *26* (7), No. 075701.

(19) Zhang, P.; Ma, L.; Fan, F.; Zeng, Z.; Peng, C.; Loya, P. E; Liu, Z.; Gong, Y.; Zhang, J.; Zhang, X.; et al. Fracture toughness of graphene. *Nat. Commun.* **2014**, *5* (1), 3782.

(20) Mortazavi, B.; Ostadhossein, A.; Rabczuk, T.; van Duin, A. C. T. Mechanical response of all-MoS_2 single-layer heterostructures: A ReaxFF investigation. *Phys. Chem. Chem. Phys.* **2016**, *18* (34), 23695−23701.

(21) Jiang, J.-W.; Park, H. S. Negative Poisson's ratio in single-layer black phosphorus. *Nat. Commun.* **2014**, *5* (1), 4727.

(22) Chen, Y.; Manna, S.; Narayanan, B.; Wang, Z.; Reimanis, I. E.; Ciobanu, C. V. Pressure-induced phase transformation in β-eucryptite: An X-ray diffraction and density functional theory study. *Scr. Mater.* **2016**, *122*, 64−67.

(23) Cherukara, M. J.; Narayanan, B.; Kinaci, A.; Sasikumar, K.; Gray, S. K.; Chan, M. K.Y.; Sankaranarayanan, S. K. R. S. Ab initio-based bond order potential to investigate low thermal conductivity of stanene nanostructures. *J. Phys. Chem. Lett.* **2016**, *7* (19), 3752−3759.

(24) Chen, Y.; Manna, S.; Ciobanu, C. V.; Reimanis, I. E. Thermal regimes of Li-ion conductivity in β-eucryptite. *J. Am. Ceram. Soc.* **2018**, *101* (1), 347−355.

(25) Jiang, J.-W.; Zhou, Y.-P. Parameterization of Stillinger-Weber potential for two-dimensional atomic crystals. *arXiv Preprint (Condensed Matter: Materials Science)*, 2017. arXiv: 1704.03147. https://arxiv.org/abs/1704.03147

(26) Xiao, H.; Shi, X.; Hao, F.; Liao, X.; Zhang, Y.; Chen, X. Development of a transferable reactive force field of P/H systems: Application to the chemical and mechanical properties of phosphorene. *J. Phys. Chem. A* **2017**, *121* (32), 6135−6149.

(27) Chen, Y.; Shi, X.; Li, M.; Liu, Y.; Xiao, H.; Chen, X. Strain and defect engineering on phase transition of monolayer black phosphorene. *Phys. Chem. Chem. Phys.* **2018**, *20* (34), 21832−21843.

(28) Deringer, V. L.; Caro, M. A.; Csanyi, G. A general-purpose machine-learning force field for bulk and nanostructured phosphorus. *Nat. Commun.* **2020**, *11* (1), 5461.

(29) Manna, S.; Hernandez, A.; Wang, A.; Lile, P.; Liu, S.; Mueller, T. A Database of Low-Energy Atomically Precise Nanoclusters. *ChemRxiv Preprint (Materials Chemistry)*, 2021. DOI: 10.26434/chemrxiv-2021-0fq3q.

(30) Natarajan, S. K.; Caro, M. A. Particle swarm based hyper-parameter optimization for machine learned interatomic potentials. *arXiv Preprint (Condensed Matter: Materials Science)*, 2020. arXiv:2101.00049. https://arxiv.org/abs/2101.00049.

(31) Wu, S.; Angelikopoulos, P.; Papadimitriou, C.; Moser, R.; Koumoutsakos, P. A hierarchical Bayesian framework for force field selection in molecular dynamics simulations. *Philos. Trans. R. Soc. A* **2016**, *374* (2060), 20150032.

(32) Henkelman, G.; Uberuaga, B. P.; Jonsson, H. A climbing image nudged elastic band method for finding saddle points and minimum energy paths. *J. Chem. Phys.* **2000**, *113* (22), 9901−9904.

(33) Henkelman, G.; Jonsson, H. Improved tangent estimate in the nudged elastic band method for finding minimum energy paths and saddle points. *J. Chem. Phys.* **2000**, *113* (22), 9978−9985.

(34) Stukowski, A. Visualization and analysis of atomistic simulation data with OVITO—The Open Visualization Tool. *Modell. Simul. Mater. Sci. Eng.* **2010**, *18* (1), 015012.

(35) Loeffler, T. D.; Manna, S.; Patra, T. K.; Chan, H.; Narayanan, B.; Sankaranarayanan, S. Active Learning A Neural Network Model For Gold Clusters & Bulk From Sparse First Principles Training Data. *ChemCatChem* **2020**, *12* (19), 4796−4806.

(36) Behler, J.; Parrinello, M. Generalized neural-network representation of high-dimensional potential-energy surfaces. *Phys. Rev. Lett.* **2007**, *98* (14), 146401.

(37) Bartok, A. P.; Payne, M. C.; Kondor, R.; Csanyi, G. Gaussian approximation potentials: The accuracy of quantum mechanics, without the electrons. *Phys. Rev. Lett.* **2010**, *104* (13), 136403.

(38) Sankaranarayanan, S.; Manna, S.; Loeffler, T.; Batra, R.; Banik, S.; Chan, H.; Sasikumar, K.; Sternberg, M.; Peterka, T.; Cherukara, M.; et al. Learning in Continuous Action Space for Determination of High Dimensional Potential Energy Surfaces. *Research Square Preprint (Materials Chemistry)*, 2021. DOI: 10.21203/rs.3.rs-284625/v1.

(39) Nelder, J. A.; Mead, R. A simplex method for function minimization. *Conput. J.* **1965**, *7* (4), 308−313.

(40) Plimpton, S. Fast parallel algorithms for short-range molecular dynamics. *J. Comput. Phys.* **1995**, *117* (1), 1−19.